Dalton Transactions

Modulating Absorption and Charge Transfer in Bodipy-Carbazole Donor-Acceptor Dyads through Molecular Design

Journal:	*Dalton Transactions*
Manuscript ID	DT-ART-01-2019-000094.R2
Article Type:	Paper
Date Submitted by the Author:	14-May-2019

Complete List of Authors:	Strahan, John; Amherst College, Department of Chemistry Popere, Bhooshan; University of Massachusetts Amherst, Chemistry Khomein, Piyachai ; University of Massachusetts, Department of Chemistry Pointer, Craig; Lehigh University, Department of Chemisry Martin, Shea; Lehigh University, Department of Chemisry Oldacre, Amanda ; Lehigh University, Department of Chemisry Thayumanavan, S; University of Massachusetts Amherst, Chemistry Young, Elizabeth; Lehigh University, Department of Chemisry

Journal Name

ARTICLE

Modulating Absorption and Charge Transfer in Bodipy-Carbazole Donor-Acceptor Dyads through Molecular Design

Received 00th January 20xx,
Accepted 00th January 20xx

DOI: 10.1039/x0xx00000x

www.rsc.org/

John Strahan[a], Bhooshan C. Popere[b,d], Piyachai Khomein[b], Craig Pointer[c], Shea Martin[c], Amanda N. Oldacre[c], S. Thayumanavan[b]*, Elizabeth R. Young[c]*

Three Bodipy-based (BDP = 4,4-difluoro-4-bora-3a,4a-diaza-s-indacene) donor-acceptor dyads were designed and synthesized, and their ground-state and photophysical properties were systematically characterized. The electronic coupling between the BDP chromophore and an electron-donating carbazole (Carb) moiety was tuned by attachment *via* the *meso* and the *beta* positions on the BDP core, and through the use of various chemical linkers (phenyl and alkynyl) to afford *meso*BDP-Carb, *meso*BDP-*phen*-Carb, and *beta*BDP-*alk*-Carb. *Meso*-substituted dyads were found to retain ground-state absorption features of the unsubstituted BDP. However, variation of the linkage between the donor and acceptor moieties modulated the photophysical behavior of excited-state deactivation by controlling the rate of photoinduced internal charge transfer (ICT). The *beta*-substituted dyad dramatically tuned (red shifted) the absorption spectrum, while retaining desired features of the BDP, specifically stability and high extinction coefficients, however the ICT kinetics were accelerated compared to the *meso*-substituted dyads. Density functional theory (DFT) and time-dependent DFT (TDDFT) were carried out on the six potential dyads formed between BDP and Carb (attachment using the *beta* and *meso* positions for all three connections: direct, phenyl and alkynyl) to support the experimental observations. DFT and TDDFT showed molecular orbital density spread across the HOMO level only when attachment occurred through the *beta* position of BDP. In the *meso*-substituted BDP-Carb dyads, the molecular orbitals resembled those of the unsubstituted BDP. This work reveals several possible synthetic paradigms to tune photophysical properties with directed synthetic modifications and provides a mechanistic understanding of the ground- and excited- state behavior in these small-molecule donor-acceptor dyads.

Introduction

Small-molecule donor-acceptor (D-A) constructs have received much attention over the last several decades as a compelling paradigm for solar energy harvesting and charge separation for energy-conversion reactions relevant to solar cells that directly produce electricity and to photoelectrochemical cells that drive chemical reactions to generate solar fuels.[1] To design useful systems for solar energy conversion, several design features must be considered including chemical- and photo-stability, high extinction coefficients, and the ability to chemically modify photo-physical properties *via* synthetic alteration. Small-molecule organics and D-A systems are attractive candidates in this regard owing to several inherent advantages: (i) they can be reproducibly synthesized and purified, (ii) they can be chemically tailored to modulate their electrochemical and optical properties, and (iii) they can be interfaced with, and incorporated into, a variety of device constructs aimed at a host of applications.[2,3,4] A wide range of molecular building blocks have been employed to construct D-A systems including porphyrins, perylene, pyrene, perylene diimides, triarylamines and many others.[5–10] However, it is necessary to expand available building blocks for D-A systems with an eye towards the critical design features noted above.

Bodipy (BDP)-based (BDP = 4,4-difluoro-4-bora-3a,4a-diaza-s-indacene) dyes comprise an important class of molecular building blocks for D-A systems. BDP dyes have been extensively studied, since their first report in 1968[11] owing to their strong molecular absorption in the visible region, high fluorescence quantum yields, excellent stability and rich redox chemistry.[12] Molecular structure in BDP-based moieties can be varied in several ways, including *via* attachment to the BDP core at various sites on the macrocycle, such as the *meso*- or *beta*-positions.[13,14] BDP moieties have been incorporated into molecular constructs in which they have served as facile charge generation components[15–24] as well as a host of other D-A systems for both charge and energy transfer[25–30].

Efforts to increase the utility of these molecular building blocks are critical. In D-A systems, the influence of molecular structure should be understood in the context of how it controls

[a] Department of Chemistry, Amherst College, Amherst, Massachusetts 01002, USA. Fax: +1-413-542-2735.
[b] Department of Chemistry, University of Massachusetts, Amherst, Massachusetts 01003, USA. E-mail:thai@chem.umass.edu; Fax: +1-413-545-4490.
[c] Department of Chemistry, Lehigh University, Bethlehem, Pennsylvania 18015, USA. Email: ery317@lehigh.edu; Fax: +1-610-758-6536.
[d] Current address: DuPont Electronics & Imaging, 455 Forest St, Marlborough, MA 01752

Electronic Supplementary Information (ESI) available: Materials and synthetic procedures, additional absorption and emission data, electrochemistry voltammograms, time-resolved emission data and DFT molecular orbital energy levels. See DOI: 10.1039/x0xx00000x

charge separation and recombination and the rates at which these processes occur. D-A interactions are known to occur through a wide range of bridges that join the donor and acceptor moieties. Direct-, alkynyl-, and phenylene-linkages, as well as many others, have been utilized to link molecular donor-acceptor systems.[8,31–37] The nature of the bridge controls the coupling between the donor and acceptor moiety, impacting any charge transfer process expected between the two moieties.[38–43] This electronic coupling has been shown to depend on, among other things, the electronic density on bridges connecting donor and acceptor systems, as well as the cant angle between the bridge units and the donor and acceptor moieties.

Directed programming of molecular characteristics can be further explored to elucidate strategies for tuning desired

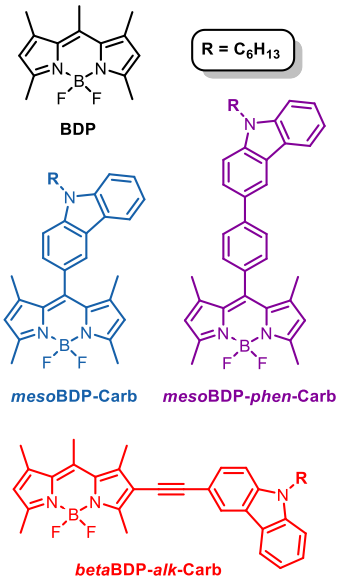

Figure 1. Structures of BODIPY (BDP)-Carbazole (Carb) dyads.

properties such as the absorption spectrum. For example, a great deal of interest has been directed at tuning the absorption spectra of desirable chromophores into redder regions of the spectrum. Tuning absorption to the red is important both for applications like solar energy conversion (where the solar flux is higher and much of the Sun's spectrum can be absorbed) as well as biomedical applications such as photodynamic therapy, which requires absorption in redder regions of 650 – 850 nm within the therapeutic window.

Enhancing the ability of BDP-based molecules to absorb in the low energy region is achieved by manipulating the frontier orbitals.[2,3,13] An extended, red-shifted spectrum may be achieved through creation of intramolecular D-A interactions between BDP and another molecular building block that is either electron rich or electron poor relative to the BDP moiety.[44] Further, attaching the molecular building block at different locations on the BDP macrocycle (specifically at the *beta* positions) enhances electronic communication between BDP and the adjoining moiety that furnishes additional red shifts to the spectrum. Lower lying LUMO levels formed from these types of interactions modulate the electrochemical redox potentials of the dyads and generate red-shifted absorption.[45] The lessons learned from these fundamental studies bring researchers much needed information in designing the next generation of molecules critical to society.

In this work, BDP serves as the foundation for creating several D-A dyads that are used to gain intuition about the influences of chemical substitution on excited-state properties. Several sites on the BDP core can be accessed synthetically to explore the influence of various chemical attachments. Of primary interest in this work is the attachment of an electron-donating carbazole (Carb) moiety onto either the *beta* or the *meso* positon of BDP.

The Carb moiety has been used in conjunction with BDP in past reports for a wide range of purposes[28,45–61]. In this study, Carb is selected as an electron-rich donor due to its lower oxidation potential compared with the BDP core, thereby ensuring sufficient driving force for photo-induced electron transfer. Carb absorption, which occurs in the 300–400 nm region, is well separated from BDP absorption, ensuring that selective excitation of the BDP core can be achieved. Further, the appended-carbazole systems produce carbazole-based radical cations with spectral signatures over a wide wavelength range (611 nm – 1000 nm) that are well-separated from expected absorption of BDP-based radical anions, thereby making them excellent handles for verifying charge transfer reactions independently from the spectroscopic handles for the BDP cation. Carb has been utilized in a range of donor-acceptor systems and in optoelectronic applications.[46,62,63]

The Carb is attached either directly to the BDP core, or *via* a phenyl or alkynyl spacer unit. An attempt was made to create a suite of dyads, in which each attachment method (direct linkage, phenyl spacer, and alkynyl spacer) was used to connect Carb to the *meso* and *beta* positions. However, synthetic challenges and molecular stability prevented the accomplishment of this effort. The dyads shown in Figure 1 represent the sub-set of molecules that proved synthetically accessible. This subset of D-A molecules provides several important insights about the relationship between the structure and photophysical properties of this class of BDP-Carb dyads. UV-visible absorption and steady-state photoluminescence collected as a function of solvent polarity are used, with the results of transient absorption spectroscopy, to determine that photoinduced intramolecular charge transfer (ICT) occurs within these dyads, and that the nature of the ICT is heavily modulated by the nature of the BDP-Carb attachment and solvent polarity. Additionally, quantum yields are determined for each dyad. Electrochemistry is used to measure oxidation and reduction potentials of each dyad, and spectroelectrochemistry is used to collect the absorption of the radical anion of the BDP-based dyads that is used to verify the formation of charge transfer products. Density functional theory (DFT) and time-dependent DFT (TDDFT) calculations are used to explain experimentally-determined trends. Time-resolved photoluminescence and transient absorption (TA) spectroscopy are used to characterize the photophysical properties of the BDP-Carb dyads.

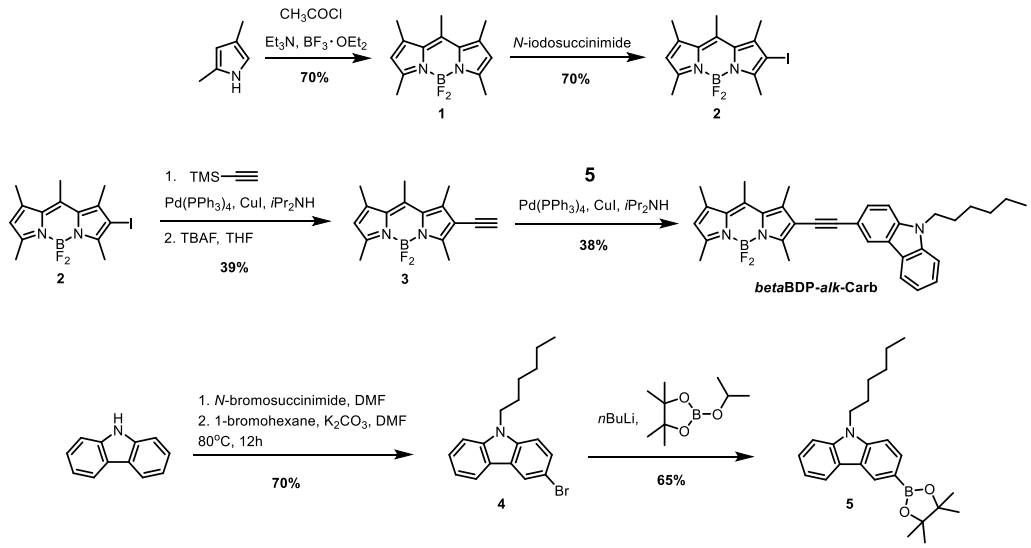

Scheme 1. Synthesis of BDP, Carb and *beta*BDP-*alk*-Carb

Experimental

Materials. Acetonitrile (ACN) and toluene used in steady-state spectroscopic studies were dispensed from a solvent system and used in ambient conditions for sample preparation. Solvents for electrochemistry and time-resolved spectroscopy were dispensed from the solvent system using air-free techniques and transferred to an inert glovebox, where sample preparation was undertaken. All reagents and starting materials were obtained from Sigma-Aldrich and used as received unless noted otherwise.

Synthesis. The synthetic routes to all the molecules are outlined in Schemes 1 and 2. As shown in Scheme 1, *meso*-methyl BDP (1) was synthesized in decent yield by the condensation of 2,4-dimethylpyrrole with acetyl chloride. The condensation product was then treated with $BF_3{\cdot}OEt_2$ to assemble the final BDP core. This core was then selectively iodinated using *N*-iodosuccinimide to afford the mono-iodo BDP, 2, in 70% yield, followed by a Pd(0) and Cu(I)-mediated Sonogashira cross-coupling reaction with trimethylsilyl acetylene. The trimethylsilyl group was deprotected using TBAF to afford the mono-ethynyl BDP (3), which was subsequently reacted with 3-bromocarbazole (4) *via* the Sonogashira coupling reaction to afford *beta*BDP-*alk*-Carb.

Analogously, *meso*-substituted BDP derivatives were obtained *via* the condensation reaction of the pyrrole with the corresponding aldehydes. Specifically, Scheme 2 shows a direct condensation reaction between 2,4-dimethylpyrrole and carbazole-3-carbaldehyde (6) afforded *meso*BDP-Carb in 20% yields with the crystal structure shown in Figure S1. Similarly, *meso*BDP-*phen*-Carb was synthesized by a Pd(II)-mediated Suzuki cross-coupling reaction between the bromophenyl-substituted BDP (7) and the carbazole boronate ester (5) in modest yield. The detailed synthetic protocol can be found in the Supporting Information.

Steady-state UV-visible and emission spectroscopy. UV-visible absorption spectra were obtained on a Perkin-Elmer Lambda 9 spectrometer with a Lambda 19 upgrade. Aliquots of 4 nmol of each moiety were reconstituted in 2 mL of solvent and used for UV-visible spectroscopy. Samples were prepared under ambient conditions at approximately 2 µM such that the optical density of each sample was kept below 1 AU for each UV-visible spectrum in a 1-cm cuvette. Fluorescence spectra were obtained on an ISS Chronos BH fluorescence lifetime spectrometer with a steady-state upgrade at an excitation wavelength of 450 nm.

Quantum yields were calculated using fluorescein as a reference fluorophore wherein, all quantum yield measurements were carried out at low concentration (optical density less than 0.075 AU in a 1-cm cuvette, ~0.1 µM) to limit reabsorption of emitted light. UV-visible spectra for quantum yield calculations were acquired on a Cary 5000 UV-vis spectrometer. Quantum yields were calculated using the following equation:

$$\varphi_{sample} = \frac{I_{sample} A_{reference} n^2_{sample}}{I_{reference} A_{sample} n^2_{reference}} \varphi_{reference},$$

where I is the integrated fluorescence intensity, A is the optical density at the wavelength used for excitation (470 nm for the reported values), and η is the index of refraction of the solvent. All experiments were performed in a 1-cm quartz cuvette. The fluorescein standard was prepared in 0.10 M NaOH, in which fluorescein has a QY of 0.91 ± 0.05.[64] Quantum yields represent the average of three trials in both acetonitrile and toluene.

Electrochemistry. All electrochemical measurements were recorded on a CH Instruments potentiostat/galvanostat. Cyclic voltammetry (CV) and differential pulse voltammetry (DPV) measurements were performed using a platinum disk (2-mm diameter) working electrode, a platinum wire counter electrode, and a silver wire quasi reference electrode, with

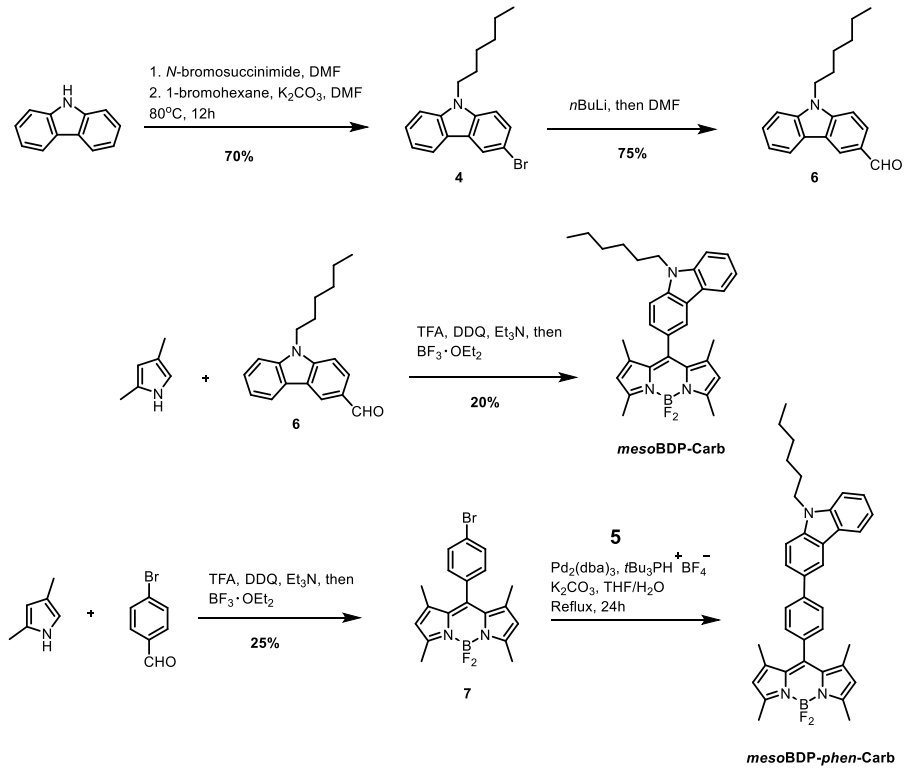

Scheme 2. Synthesis of *meso*BDP-Carb and *meso*BDP-*phen*-Carb

0.1 M tetrabutylammonium tetrafloroborate ($TBABF_4$) as the supporting electrolyte in acetonitrile. All experiments were performed with an analyte concentration of 60 µM. Sample preparation and electrochemical measurements were carried out in an inert glovebox environment. After the experiment was performed, ferrocene (Fc) was added as in internal standard. All redox potentials are reported relative to the Fc/Fc^+ couple. The scan rate for the CV experiments was 0.1 V/s. DPV was performed with a pulse period of 0.5 s, a sample width of 0.167 s, and an amplitude of 0.5 V, in increments of 0.004 V. Scans were recorded between 1.5 and −1.5 V.

Time-resolved fluorescence. Time-resolved photoluminescence measurements were taken on an ISS Chronos BH lifetime spectrometer using time-correlated single photon counting. A 470 nm pulsed LED light source with a pulse duration of ~20 ns was used to excite the sample. A 470 nm bandpass filter was used to filter the excitation pulse, and a 500 nm longpass filter was used in the emission channel to remove scattered LED light from the sample emission. The entire emission spectrum was integrated to produce the emission decay trace. The instrument response was collected without the 500 nm longpass filter using a scattering solution of coffee creamer in water. Samples were prepared in an inert glovebox environment in a 1-cm quartz cuvette, and kept at low concentration. The cuvettes were sealed to preserve an air-free sample and removed from the glovebox for experiments. Measurements were collected in acetonitrile and toluene. Lifetimes were extracted by fitting a convolution of the instrument response and a multiexponential decay to the data using ISS Vinci2 software.

Spectroelectrochemistry. Spectroelectrochemical measurements were recorded with a CH Instruments potentiostat/galvanostat and a USB 2000+ Ocean Optics UV-visible spectrometer. Samples were prepared at a concentration of 30 µM in acetonitrile with a 0.1 M $TBABF_4$ electrolyte concentration and transferred to a 2-mm quartz cuvette. A platinum mesh working electrode, a silver wire reference electrode, and a platinum wire counter electrode were used. The spectroelectrochemistry cell was constructed in the 2-mm glass cuvette using cleaned and polished electrodes. The absorption spectrum was taken through the platinum mesh working electrode of the sample prior to applying any potential, then the spectrometer was blanked on the sample solution. Bulk electrolysis was used to apply potentials in 200 mV steps in order to generate the redox product. After the potential was applied, the absorption spectra were recorded once steady state was reached, usually in about 100 seconds. A series of difference absorption spectra were recorded on the oxidized or reduced sample. Fresh samples were used for each oxidative and reductive run.

Transient absorption spectroscopy. Femtosecond transient absorption spectroscopy was performed with an Ultrafast Systems Helios spectrometer. One hundred fifty femtosecond pulses of 800 nm laser light were generated with a Coherent Libra amplified Ti:sapphire system at 1.2 W and 1 kHz repetition rate. Approximately 80% of the 800 nm pulses was sent to a Topas-C optical parametric amplifier to generate a 500 nm

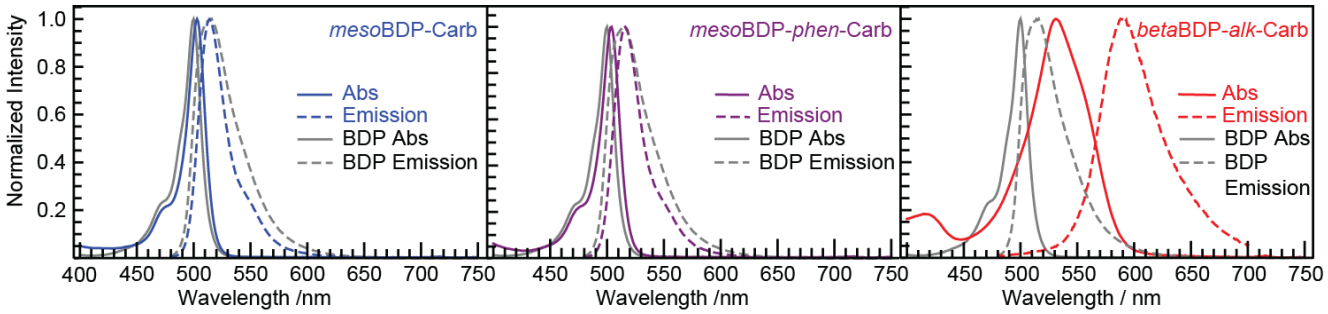

Figure 2. Normalized absorption and emission spectra for each BDP-Carb D-A dyad compared to the unmodified BDP moiety (in grey) recorded in acetonitrile. Samples for absorption were approximately 2 µM and for fluorescence were 0.1 µM. Fluorescence samples were excited at 450 nm.

pump pulse. The pump pulse was sent through a depolarizer to eliminate contributions to TA from orientational diffusion and attenuated to between 0.5 mW and 1 mW to prevent decomposition of the sample. The remainder (~20%) of the 800 nm light was sent through a sapphire crystal to generate a white light continuum for use as the probe pulse. The probe pulse was delayed on a delay stage to generate the time difference between the pump and probe. An optical chopper was used to remove every other pump pulse, and for each time delay, a series of unpumped and pumped probe pulses were recorded by the detector (a Hamamatsu S10453-1024Q Si-based detector). In each case, a reference probe pulse (that does not go through the sample) was collected and processed to improve the S/N while minimizing the number of scans needed to obtain quality data. The transient absorption spectra were measured over a 5 ns window. For each scan, 250 time points were recorded and each sample was subjected to three scans. The sample was stirred with a magnetic stir bar during every run. Samples for transient absorption spectroscopy were prepared in an inert glovebox environment in a 2-mm quartz high-vacuum cuvette. The concentration of each compound was chosen in order to have a peak optical density of about 0.4 AU. UV-visible absorption spectra were recorded before and after each TA experiment to verify that no decomposition had occurred. Solvent responses were also recorded and subtracted from the relevant spectra, and a chirp correction was applied to each data set. Lifetimes were extracted by fitting a convolution of a multiexponential decay and an instrument response function to the decay at single wavelengths. Quality of the fitting was assessed by examining the residuals and comparing the fitting results at several different wavelengths.

Computation: Density functional theory (DFT) and time-dependent density functional theory (TDDFT) were employed to further elucidate the relationship between molecular geometry, namely the manner in which molecular geometry impacts molecular orbital density, and the photophysical properties of the prepared dyads. Models were generated in GaussView 6 for all six permutations of the BDP-*linker*-Carb system.[65] Gaussian 09 was used to perform geometric and energetic calculations.[66] Calculations for DFT were performed using the B3LYP functional[67,68,69,70] and a def2-TZVP basis set[71]. Calculations for TDDFT were performed using the 6-311g (d,p) basis set.[72–75] All calculations were performed in pcm solvent model for acetonitrile.[76] Alkyl chains were replaced with methyl groups for computational simplicity.

Results

Steady-state absorption and emission. The dependence of the steady-state spectroscopic properties on the substitution pattern and the solvent polarity was investigated for the suite of BDP dyads. Figure 2 shows the absorption and emission spectra of *meso*BDP-Carb, *meso*BDP-*phen*-Carb and *beta*BDP-*alk*-Carb in acetonitrile overlaid with the emission and absorption spectra of unsubstituted BDP. The absorption wavelength maxima, Stokes shifts, and quantum yields of each species are summarized in Table 1. The small Stokes shift of BDP (7 nm, 0.0354 eV in ACN; 14 nm, 0.0675 eV in toluene) is retained in the *meso*-substituted dyads, specifically *meso*BDP-Carb (7 nm, 0.0803 eV in ACN; 11 nm, 0.0527 eV in toluene) and *meso*BDP-*phen*-Carb (8 nm, 0.0395 eV in ACN; 11 nm, 0.0525 eV in toluene). However, a significant Stokes shift is seen in *beta*BDP-*alk*-Carb (41 nm, 0.173 eV in ACN; 57 nm, 0.226 eV in

Table 1. *Summary of UV-visible Absorption and Emission Data*

	Acetonitrile				Toluene			
Molecule	**Abs/nm**	**PL/nm**	**Stokes/eV**	**QY %**	**Abs/nm**	**PL/nm**	**Stokes/eV**	**QY %**
BDP	492	499	0.0354	98(9)	500	514	0.0675	95(1)
*meso*BDP-Carb	498	505	0.0803	2.3(0.1)	503	514	0.0527	90(11)
*meso*BDP-*phen*-Carb	497	505	0.0395	0.8(0.1)	504	515	0.0525	50(9)
*beta*BDP-*alk*-Carb	522	563	0.173	1.6(0.3)	531	588	0.226	12(4)

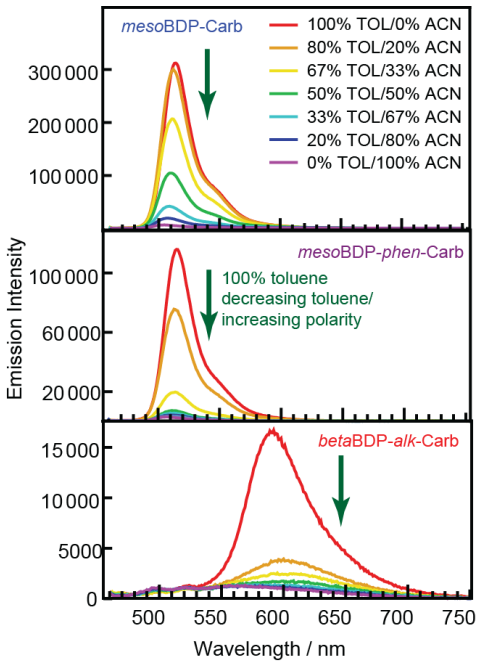

Figure 4. *Solvent polarity dependence of emission spectra of each BDP-Carb D-A moiety. Samples were 0.1 μM in the solvent ratio of toluene/acetonitrile indicated in the legend (shifting from red as the most non-polar to blue as the most polar in rainbow order). Samples were excited at 450 nm.*

toluene). In general, spectral features of the *meso*-substituted molecules resemble those of the BDP, while those of the *beta*-substituted molecule diverge significantly. Figure S2 shows absorption spectra of each BDP-Carb dyad, as well as the unsubstituted BDP and carbazole moieties, extended to the UV region. Likewise, absorption in the UV region of the spectrum reveals that absorption attributed to the carbazole portion of the dyads is modestly red shifted from the unsubstituted carbazole in the *meso*-substituted derivatives. The spectral shape of the *beta*-substituted dyad in the UV region is more substantially perturbed, obscuring the origins of the broadened peaks in that region.

Solvent polarity was found to have little effect on the intensity and shape of the absorption spectra of the BDP-Carb dyad (Figure S3), however the influence of solvent polarity on the fluorescence quantum yield of these molecules is significant (Figure 4). Increasing the solvent polarity reduces the quantum yield significantly in the BDP-Carb dyads, while it has little effect on the quantum yield of unsubstituted BDP (Table 1). The emission spectra blue shift slightly with increasing polarity as can be seen more clearly in normalized emission spectra shown in Figure S4 in the Supporting Information. The same blue shift is observed for the unsubstituted BDP (Figure S5). In the *meso*BDP-Carb dyad, a broad, weak second emission peak appears at ~600 nm in the emission spectrum with increasing solvent polarity (Figure S4). In the *beta*-substituted molecule, the general shape of the fluorescence spectrum is retained in polar solvents, and the spectrum appears blue shifted slightly in the same fashion as the meso-substituted dyads, although low signal obscures the exact nature of the change. In contrast, the emission intensity of BDP alone increases with increasing polarity (Figure S5).

Transient absorption spectroscopy and time-resolved photoluminescence. Transient absorption and time-resolved photoluminescence spectroscopy were performed on each BDP-Carb dyad in both acetonitrile and toluene. Figure 4 shows overlays of the absorption, emission, and TA spectra for the three BDP dyads in acetonitrile and toluene. Corresponding overlays of absorption, emission and TA spectra for

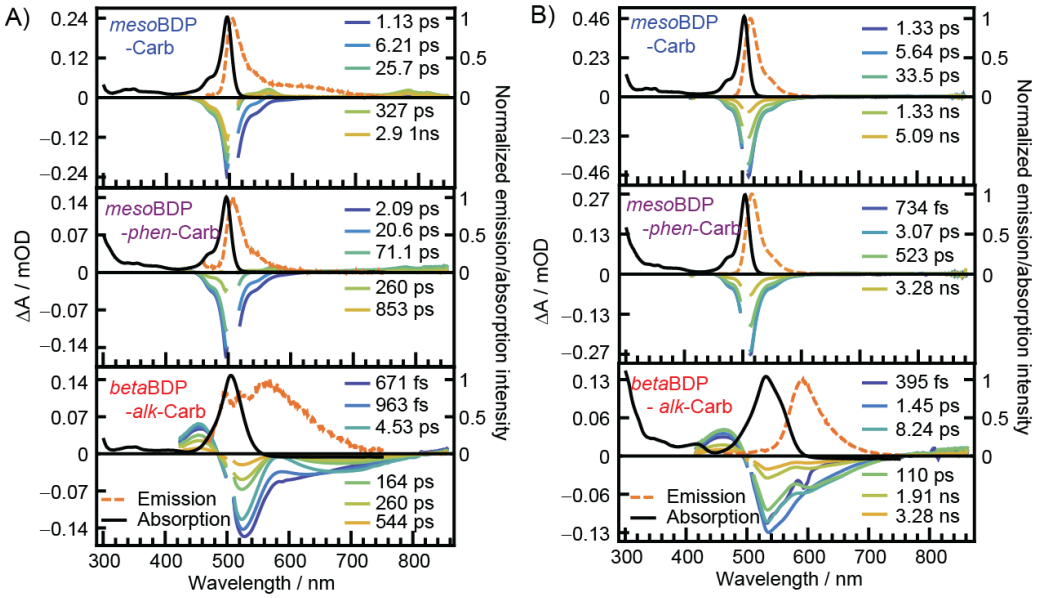

Figure 3. Overlay of transient absorption spectra with the steady-state absorption (black) and emission (orange) spectra for BDP-Carb D-A dyads in A) acetonitrile and B) toluene. Samples for TA were prepared in an inert glovebox environment in a 2-mm quartz high-vacuum cuvette to have a peak optical density of ~0.4 AU. Gaps in the spectra correspond to removal of scatter laser excitation light around 500 nm.

Table 2. *Lifetimes Obtained from Time-Resolved Emission and Transient Absorption Spectroscopy*

	Emission	Transient Absorption	
Acetonitrile	τ / ns	τ_1 /ns (error)	τ_2 /ps (error)
BDP	5.72	6.6 (1.2)	
*meso*BDP-Carb	3.25	7.52 (0.14)	5.324 (0.054)
*meso*BDP-*phen*-Carb	0.17	0.187 (0.011)	41.0 (4.9)
*beta*BDP-*alk*-Carb	0.31	0.2812 (0.0049)	1.1715 (0.0021)
Toluene	τ / ns	τ_1 /ns (error)	τ_2 /ps (error)
BDP	4.14	6.58 (0.29)	
*meso*BDP-Carb	3.50	4.001 (0.023)	85.1 (6.1)
*meso*BDP-*phen*-Carb	2.58	2.935 (0.058)	87.7 (3.1)
*beta*BDP-*alk*-Carb	2.06	1.838 (0.010)	6.03 (0.15)

Emission lifetimes indicates the lifetime obtained from the time-resolved photoluminescence experiments. The TA global analysis lifetimes are shown with the error in parenthesis, i.e. lifetime(error).

unsubstituted BDP are shown in Figures S6 and S7 in the Supporting Information. In the *meso*-substituted dyads, the TA main features include a bleach at 510 nm, and growths at 560 nm and 800 nm. The bleach at 510 nm can be assigned to the ground-state bleach, whereas the peaks at 560 nm and 800 nm grow in concurrently suggesting they represent a photo-induced product, namely a charge transfer (CT) state. Comparison with the spectroelectrochemistry (Figure 5) suggests that the growth at 560 nm can be attributed to the formation of a CT species owing to the correspondence of the TA growth at 560 nm with the radical anion absorption peak recorded upon reduction of the dyad. The main features of the *beta*BDP-alk-Carb spectrum include a bleach at 520 nm, a bleach at 680 nm, and a growth convolved with both bleaches at 590 nm. Comparison with the steady-state absorption and emission spectra suggests that the bleach at 520 nm can be assigned to bleaching of the ground state, and the broad bleach at 660 nm can be assigned to stimulated emission (*vide supra*).

Lifetimes obtained from global analysis fitting are presented in Table 2. The TA data were cropped below 540 nm to exclude scattering from the excitation pulse that complicates global analysis fitting. Therefore, the decay-associated difference spectra (DADS) represent the contributing spectra only to the red of 540 nm. The BDP-Carb dyad data were fit with two principal components, the shorter-lifetime component corresponding to formation of the charge transfer state and the longer to its decay (*vide infra*). A single component was satisfactory for fitting unsubstituted BDP. These fits resulted in the lifetimes τ_1 and τ_2 reported in Table 2.

The photoluminescence (PL) lifetime data are presented in Table 2. Each sample was fit to a single lifetime producing a good residual trace (Figure S8). The emission lifetime for each dyad in each solvent corresponds to the longer TA lifetime of that dyad, however the magnitudes do not match exactly. The shorter TA lifetimes are well below the time resolution of the instrument and could not have been resolved using that technique.

Electrochemistry and Spectroelectrochemistry. The redox properties of the BDP-Carb dyads were investigated in acetonitrile using CV and DPV and the corresponding voltammograms are shown in Figures S9 and S10 in the Supporting Information. The CV half wave potentials are summarized in Table 3. BDP and each BDP-Carb dyad shows a quasi-reversible reduction event at ~−1.6 V, and all of the dyads show an irreversible oxidation event at ~0.7 V. No reduction peak was observed for Carb.

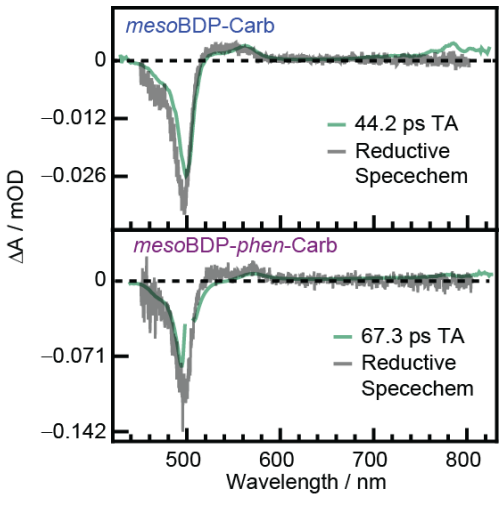

Figure 5. Comparison of TA and spectroelectrochemistry. Spectroelectrochemistry was performed using 30 μM samples of each BDP-Carb dyad in 0.1 M TBA BF_4 in acetonitrile using a platinum mesh working electrode, a platinum counter electrode, and a silver wire quasi-reference electrode.

Table 3. *Summary of Electrochemical Potentials*

Molecule	$E_{1/2}$ (ox) (V vs. Fc/Fc+)	$E_{1/2}$ (red) (V vs. Fc/Fc+)
BDP	0.74	–1.65
Carbazole	0.81	
*meso*BDP-Carb	0.73	–1.58
*meso*BDP-*phen*-Carb	0.76	–1.56
*beta*BDP-*alk*-Carb	0.64	–1.64

Cyclic voltammetry was performed using 60 μM of the analyte in 0.1 M TBA BF_4 in acetonitrile with a platinum working electrode, a platinum counter electrode, and a silver wire quasi reference electrode. Voltammetry scans were recorded using an internal ferrocene standard.

Spectroelectrochemistry was attempted for BDP, Carb and each of the BDP-Carb dyads in acetonitrile with a 0.1 M $TBABF_4$ electrolyte concentration. Reductive spectroelectrochemistry spectra were recorded for *meso*-substituted BDP-Carb dyads and are shown overlaid with TA spectra in Figure 5. In these spectra, a clear bleach of the neutral species is seen at ~510 nm convolved with the growth of a peak associated with the reduced species at ~560 nm. Figure S11 shows the reductive spectroelectrochemistry spectrum of BDP, which also reveals a peak associated with the radical anion at ~555 nm, consistent with previous reports[77], confirming the assignment of the peak at 560 nm in the *meso*-substituted BDP-Carb dyads. The reductive spectroelectrochemical signature of the *beta*BDP-*alk*-Carb remained elusive as the bleach of the neutral state was observed, but no features corresponding to the reduced species appeared. Further, oxidative spectroelectrochemistry aimed at identifying the absorption peaks associated with the radical cation of the BDP-Carb dyads did not furnish conclusive data. However, in literature, radical cation absorption peaks of various substituted carbazole molecules have been identified over a wide wavelength range (611 nm – 1000 nm).[78–80] The electrochemistry (CV alone, Figure S9) of the dyads reveals that the oxidations of the BDP-Carb dyads was quite irreversible, which may have contributed to the difficulty observing the radical cation.

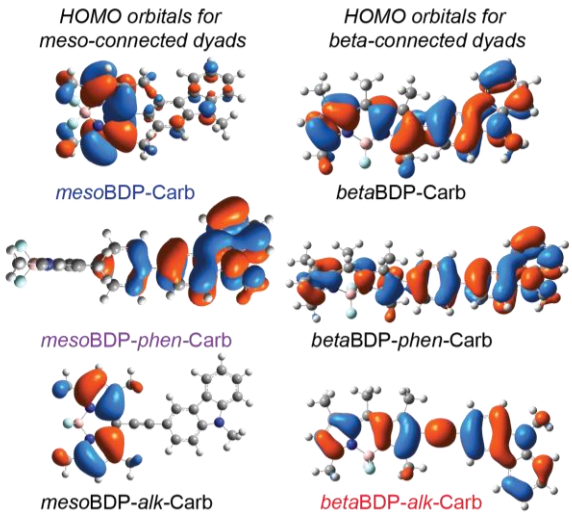

Figure 6. DFT calculated HOMO orbitals for each possible bridging unit (direct, alkynyl, phenyl) for the *beta*- and *meso*-substituted BDP-Carb dyads.

Computation. DFT calculations were used to visualize the degree of electronic coupling between the BDP and Carb moieties in the ground state and to rationalize the experimentally observed spectroscopic trends. Figure S12 and S13 show the DFT calculated HOMO-2, HOMO-1, HOMO, LUMO, LUMO+1, and LUMO+2 orbitals and tabulated and plotted orbital energy levels of synthesized *beta*BDP-*alk*-Carb and the *meso*-substituted dyads *as well as* those dyads that were not successfully isolated. Figure 6 shows the calculated HOMO orbital density for each of the six BDP-Carb dyads. The HOMOs of the *meso*-substituted dyads are localized entirely on either the BDP (*meso*BDP-Carb and *meso*BDP-*alk*-Carb) or Carb (*meso*BDP-*phen*-Carb) moiety. The HOMO-1 molecular orbitals of the *meso*-substituted dyads reside on the other moiety of dyad than the HOMO. In contrast, the HOMO and the HOMO-1 molecular orbitals of the *beta*-substituted dyads are delocalized across both the BDP and Carb moieties. These results are consistent with the experimentally observed trend that the absorption and emission spectra are broader and red shifted in *beta*BDP-*alk*-Carb compared to the *meso*-substituted dyads and suggest that these trends may be followed for the BDP-Carb dyads that were not isolated. In general, the LUMO orbitals of each computed BDP-Carb dyad are similar to each other (localized on the BDP portion of the dyad). The orbitals of the LUMO+1 energy level for the BDP-Carb dyads reside on the Carb moiety in each case.

Discussion

Using computational results to interpret modulation of absorption spectra. The calculated molecular orbitals for the *meso*-substituted BDP-Carb dyads show very little electronic coupling between the BDP and Carb moieties in the frontier molecular orbitals, which is expected because no electronic density resides on the *meso* position of unsubstituted BDP moiety. These results support the experimental observation that the UV-visible absorption spectra of the *meso*BDP-Carb and *meso*BDP-*phen*-Carb dyads very closely resemble that of the unsubstituted BDP. TDDFT predicts that the *meso*BDP-Carb and *meso*BDP-*phen*-Carb dyads undergo transitions between orbitals localized primarily on the BDP or Carb moiety in their lowest-energy electronic transitions (HOMO-1 → LUMO for *meso*BDP-Carb and HOMO → LUMO for *meso*BDP-*phen*-Carb) with low oscillator strengths, indicating negligible overlap between orbital densities of the two states. Further, TDDFT predicts that *meso*BDP-*alk*-Carb, one of the dyads that was unable to be synthetically prepared, would have an absorption spectrum that resembles those of *meso*BDP-Carb and *meso*BDP-*phen*-Carb with respect to the peak positions. However, the absorption spectrum may be broadened in

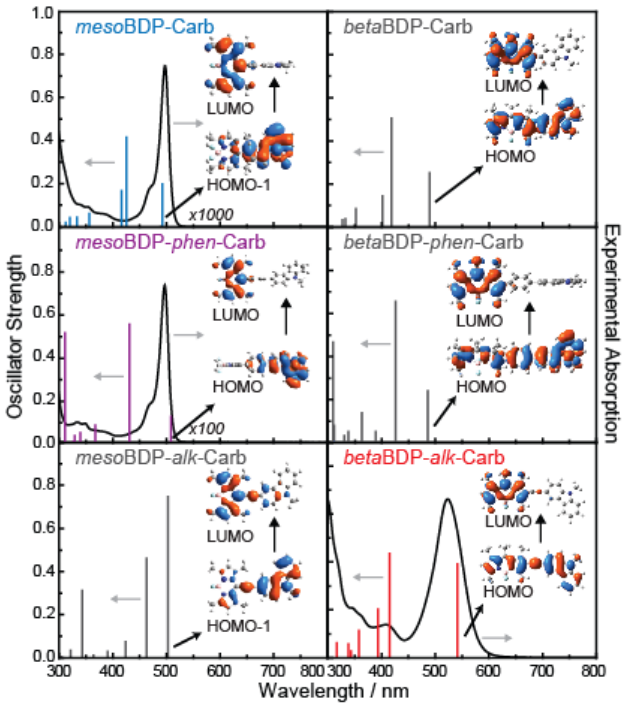

Figure 7. Predicted transitions from TDDFT, overlaid on experimental absorption spectra.

*meso*BDP-*alk*-Carb because the BDP and Carb moieties are more planar when separated by the alkynyl spacer and the orbitals associated with the lowest-energy transition (HOMO-1 and LUMO) are more delocalized, leading to a substantially higher calculated oscillator strength.

The experimentally-observed absorption spectrum of the synthetically prepared *beta*BDP-*alk*-Carb, on the other hand, differs dramatically from that of the unsubstituted BDP. The HOMO-2, HOMO-1 and HOMO molecular orbitals of *beta*BDP-*alk*-Carb are delocalized over the BDP and Carb moieties. This increased conjugation is expected because the BDP and Carb moieties are more planar as a result of the significant orbital density on the *beta* position of unsubstituted BDP. The significant extension of the π system in the HOMO and HOMO-1 orbitals of the *beta*BDP-*alk*-Carb dyad results in the observed red shifting and broadening of the low-energy feature in its UV-visible absorbance spectrum (522 nm). TDDFT forecasts this shift, predicting the lowest-energy transition (HOMO → LUMO) of *beta*BDP-*alk*-Carb to occur at 542 nm. This red shifting, however, is not predicted by TDDFT for *beta*BDP-Carb or *beta*BDP-*phen*-Carb. The BDP and Carb moieties in the *beta*BDP-Carb or *beta*BDP-*phen*-Carb are not planar with dihedral angles of 56.1° for *beta*BDP-Carb and 91.1° for *beta*BDP-*phen*-Carb. Accordingly, the predicted lowest-energy transitions between HOMO and LUMO occur at 490 nm for *beta*BDP-Carb and 486 nm for *beta*BDP-*phen*-Carb. Peak broadening cannot be confirmed for *beta*BDP-Carb or *beta*BDP-*phen*-Carb, but is expected based on the delocalized HOMOs and caculated oscillator strengths.

In general, the results from DFT and TDDFT provide insight into the trends observed across the absorption spectra of BDP and the BDP-Carb dyads, which allows for greater predictability and tunability in this class of compounds.

Spectroelectrochemistry to identify spectral signatures of CT products. Cyclic voltammetry clearly reveals that most redox events are irreversible. It is therefore more reliable to use differential pulse voltammetry to determine the redox potentials of each dyad. All BDP-Carb dyads show an irreversible reduction event at around −1.6 V vs Fc/Fc^+ as shown in Figure S9. Since Carb has no reductive event in this potential window, this reduction likely corresponds to the addition of an electron to the BDP portion of the dyad. Both BDP and Carb have an irreversible oxidation at 0.74 V and 0.882 V vs Fc/Fc^+, respectively and therefore the origin of the oxidation is not immediately clear. We can gain further insight into the electrochemical origins of the redox peaks from inspection of the Kohn-Sham orbitals obtained from DFT (Figure S12). Oxidation corresponds to removing an electron from the HOMO, and therefore, reflects the energy of the HOMO. In the *beta*-substituted dyad, the HOMO is delocalized across the entire molecule, so the resulting radical cation corresponds to neither the BDP nor Carb radical cations since the positive charge is delocalized across the entire molecule. For the *meso*-substituted dyads, since the HOMO is localized on the BDP moiety, oxidation of these molecules can plausibly correspond to the formation of a BDP radical cation. Since only the reductive redox event can be conclusively assigned to one component of the dyad, reductive spectroelectrochemistry is used to identify the spectral signatures of a CT state involving a reduced BDP.

Excited-state formation and deactivation. The solvent-dependent steady-state absorption and emission spectra of each dyad were recorded in toluene, acetonitrile, and mixtures of the two solvents. The absorption spectra are largely invariant with solvent polarity, while the intensity of the emission spectra vary significantly. The different solvent dependencies likely signify that emission is quenched as the ICT pathway is turned on in more polar solvents. Analysis of the solvent-dependent emission spectra in Figure 4, Figure S4 and Figure S5 reveals that while the emission peak corresponding to the local excited state (at ~505 nm in acetonitrile and ~515 nm in toluene) decreases in intensity, a clear emission peak corresponding to a new state, such as a charge transfer (CT) state is not observed, since emission from a CT state would be expected to appear to the red of the local excited-state emission. In the case of *meso*BDP-Carb, a very small, broad and red-shifted peak can be discerned at ~625 nm, however this peak does not contribute significantly to the experimental spectra. Further, were an internal CT state to emit, the emission peak would be expected to red shift with increasing solvent polarity. The observed primary emission peak, however, does not shift to a great extent, and what shift does occur is small and blue shifted with increasing solvent polarity. In fact, the unsubstituted BDP emission (Figure S5) shows a similar, small blue shift with increasing solvent polarity. These data suggest by way of comparison and with insight from

the Lippert equation[81] that the change in dipole moment between the emissive state and the ground state is small and further imply that the observed emission occurs from the S_1 state and not the CT state.

Transient absorption spectroscopy to characterize CT formation. TA was used to determine the presence and evaluate the dynamics of transiently formed species after photoexcitation of the BDP-Carb dyads. Figure 4 (and S6 and S7) shows TA spectra and Figure 8 (and S13) shows the results of global analysis fitting of the BDP-Carb dyads (and unsubstituted BDP) in acetonitrile and toluene.

Transient absorption spectra. In acetonitrile, the TA spectra bleach at ~515 nm corresponds to the ground state depopulation. Further, the *meso*-substituted dyads show a growth at 560 nm that overlaps with the reductive spectroelectrochemistry peak corresponding to the BDP radical anion and leads to the assignment of this TA peak as the growth of the CT state. In *beta*BDP-*alk*-Carb, a ground-state bleach is observed in the TA spectra at 570 nm and a stimulated emission bleach is observed in a broad peak ~700 nm. A positive going signal, convolved with the broad bleach peaks is observed at 580 nm and assigned to the formation of a CT state in the *beta*BDP-*alk*-Carb dyad.

In toluene, similar features were observed for *beta*BDP-*alk*-Carb, however, the 570 nm and 700 nm bleach peaks were narrower and the CT peak is much less prominent. The *meso*-substituted dyads in toluene also show a smaller TA signal at 570 nm compared to the *meso*-substituted dyads in acetonitrile. Based on the TA spectra, it is unclear if CT occurs at all for the *meso*-substituted dyads in toluene. These observations are consistent with the assignment of the peaks at ~570 nm to a CT state. Indeed, while the CT peaks are observed in more polar solvent, the peaks are smaller or even disappear in the less polar solvents that disfavour charge transfer.

Global Analysis Fitting. To further understand the nature of the excited-state deactivation, global analysis was performed. Figure 8 and Figure S14 show the results of global analysis fitting. Unsubstituted BDP contains only one contributing component resulting in a single DADS, namely the ground-state bleach recovery (Figure S14). The ground-state bleach recovery occurred on the order of ~6.7 ns in both acetonitrile (6.6 ns) and toluene (6.85 ns).

The global analysis fitting of the BDP-Carb dyads reveals differing photophysical processes in the two solvents. In acetonitrile, DADS indicate that a photo-induced CT state is formed. The fitting of the BDP-Carb dyads TA spectral data identified two contributing DADS, with one corresponding to the formation of a CT state and the other corresponding to the disappearance of that state (*i.e.* recovery of the ground state). In acetonitrile, each shorter-lifetime DADS (red, dashed) shows distinct negative-going features at ~560 and ~780 nm (the feature at ~780 nm is likely red shifted and cut off for the *beta*-substituted dyad), that represent the formation of the CT state. The longer-lifetime DADS (green, solid) appears as a mirror image of the shorter-lifetime DADS, indicating that the longer-lifetime DADS is formed from the shorter-lifetime DADS and therefore represents the decay of the CT state back to the ground state. The large negative-going signal at 560 nm in the shorter-lifetime DADS corresponds to the formation of the BDP radical anion, supported by the results obtained with spectroelectrochemistry of the *meso*-substituted dyads (*vide supra*). While definitive spectral confirmation of the radical anion for *beta*BDP-*alk*-Carb was not obtained with

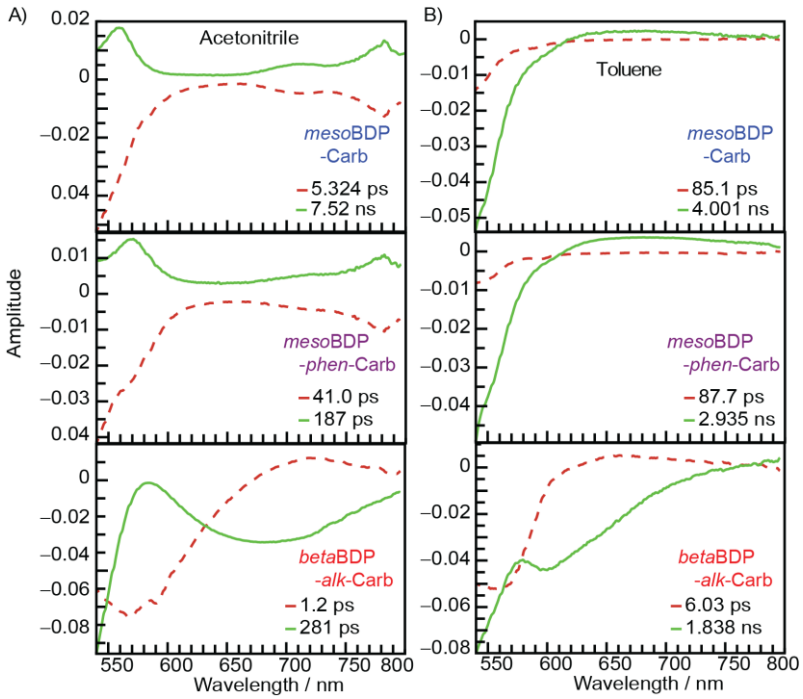

Figure 8. Global analysis DADS of transient absorption measurements for BDP-Carb D-A dyads in A) acetonitrile and B) toluene.

spectroelectrochemistry, assignment of the peak is founded on the following: (i) BDP (Figure S11) and the *meso*-substituted dyads reveal a radical anion peak slightly red shifted from the BDP-based ground-state absorption peak, and (ii) the 580 nm TA growth (Figure 4) appears red shifted and broader in a similar fashion to that of the steady-state *beta*BDP-*alk*-Carb absorption. Thus, the proposal that each of the negative-going features in the shorter-lifetime DADS at ~560 nm (at 560 nm for the *meso*-substituted dyads and at 580 nm for *beta*BDP-*alk*-Carb) is the CT peak represents a highly plausible assignment. The negative-going signal in the shorter-lifetime DADS at 780 nm likely corresponds to the formation of the Carb radical cation. As mentioned above, literature reports of the carbazole radical cation peak have been reported over a wide wavelength range (611 nm – 1000 nm) and observation of the feature at 780 nm is consistent with this assignment.[78–80]

In contrast, the global analysis DADS in toluene do not conclusively indicate that a photo-induced CT state is formed. The DADS features associated with the radical anion and cation are less intense or not observed at all in the shorter-lifetimes DADS in toluene compared to the shorter-lifetime DADS produced by fitting the acetonitrile data. For example, for *beta*BDP-*alk*-Carb, the negative-going peak in the shorter-lifetime DADS near 560 nm corresponding to the BDP radical anion is less prominent. The feature corresponding to the Carb radical cation is, however, likely obscured for the same reason it is not observed in the acetonitrile DADS (red shifting of the peak in the more highly-conjugated dyad). As is the case for the DADS produced for the acetonitrile data, the longer-lifetime DADS for *beta*BDP-*alk*-Carb in toluene is roughly a mirror image of the shorter-lifetime DADS (specifically the positive-going feature at ~560 nm), thereby representing the decay of the lower-yielded CT state. Because the radical anion and cation features are significantly less intense in toluene, the longer-lifetime DADS resembles the unsubstitued BDP DADS shown in Figure S14.

For the *meso*-substituted dyads in toluene, both the radical anion and cation features are less intense in the short-lifetime component leading to uncertainty in assigning this DADS to formation of the CT state. Of note is that the longer-lifetime DADS for the BDP-Carb dyads (~2-4 ns) in toluene is quenched compared to unsubstituted BDP DADS (~6.6 ns) indicating either that some amount of CT may in fact be contributing to depletion of the excited state or that rotation of the appended Carb group facilitates faster non-radiative decay of the BDP moiety. The *meso*-substituted BDP-Carb dyads DADS corresponding to the CT states (the shorter-lifetime DADS) have similarly shaped DADS to one another in the same solvent. However, in toluene, the lifetime that corresponds to the potential CT state formation is longer at > 80 ps compared to the DADS of the same dyad in acetonitrile, which produced a CT state formation lifetime of < 45 ps. The same observation is true for the *beta*-substituted BDP-Carb dyads in which the lifetime of DADS corresponding to formation of the CT state in acetonitrile is 5 times shorter than toluene.

In acetonitrile, the amplitudes of the CT-state DADS are significantly more intense than those in toluene, suggesting that CT occurs with a higher yield in acetonitrile than in toluene. This result is expected as ET is anticipated to be faster and occur with greater yield in the more polar solvent, acetonitrile, compared to the less polar solvent, toluene. Furthermore, the *beta*-substituted dyads show a greater yield than the *meso*-substituted dyads in the same solvent, suggesting that the *beta*-substituted dyads, with their increased electronic coupling, lead to more significant formation of CT state compared to the *meso*-substituted dyads.

Nature of the Excited State. The results of the solvent-dependent emission and spectroelectrochemistry, in conjunction with the TA data, suggest that a photoinduced, non-emissive ICT state is formed in these BDP-Carb dyads rather than a directly excited CT state. The CT state is formed more readily in polar solvents than in non-polar solvents, as would be expected for photo-induced CT. This assignment arises from the observation that the absorption and emission spectra do not shift significantly as a function of solvent polarity, while the emission spectra are highly quenched with increasing solvent polarity. These observations are indicative of formation of a state that is not directly excited. Further, TA spectroscopy shows a peak assigned to the CT state that grows in on fast times scales and then decays as the ground state is recovered. Taken together, the assignment of photoinduced ICT in these BDP-Carb dyads is a reasonable one.

Tuning photophysics through chemical modification. The chemical and photophysical nature of the dyads are tuned through the use of various chemical attachments (direct, phenyl spacer, alkynyl spacer) at different positions on the BDP macrocycle. Several observations may be formulated from these results. First, significant perturbation of the frontier molecular orbitals can be achieved to tune the ground-state properties, particularly the absorption spectrum. The *beta*-*alkynyl*-substituted dyad possesses a dramatically red-shifted and broader ground-state absorption than the parent BDP moiety. DFT was used to identify that the observed spectral features derive from changes to the HOMO and HOMO-1 molecular orbitals, both of which showed electron density delocalized over both the BDP and Carb moieties. However, based on DFT, a direct or phenyl linkage *via* the *beta* positon would not be predicted to cause significant red-shifting, although broadening of the peak is predicted. In contrast, the *meso*-substituted dyads retain ground-state properties similar to those of the parent BDP molecule. The lack of orbital density on the *meso* position of unsubstituted BDP was retained in both *meso*-substituted dyads. The addition of the phenyl spacer did not extend the molecular orbitals calculated *via* DFT from the BDP moiety towards the Carb moiety.

Comparison of the directly-linked and phenyl-linked *meso*-substituted BDP-Carb dyads reveal that ICT was ~8 times faster in the directly-linked dyad than in the phenyl-spaced dyad in acetonitrile. The ICT state was longer-lived in the directly-linked *meso*BDP-Carb dyad than in *meso*BDP-*phen*-Carb. The angle between the BDP and Carb slows the back charge transfer rate for

the directly-linked dyad. In contrast, rotation of phenyl group in *meso*BDP-*phen*-Carb may have changed in the ICT state compared to the ground state of that dyad, resulting in faster back electron transfer. The differences between the DADS-produced lifetimes for the *meso*-substituted BDP-Carb dyads was less pronounced in toluene, further indication that this process may not be due to ICT.

ICT was clearly tuned as a function of attachment positions (*meso* or *beta*) and spacer used (direcly-connected, phenyl spacer, or alkynyl spacer). These conclusions are made via observation of the ICT rates in each dyad and yields as the solvent polarity is modulated from the more polar solvent, acetonitrile, to the less polar solvent, toluene (*vide supra*). These conclusions are: (1) CT is more facile (faster and higher yielding) when BDP and Carb are attached *via* the *beta* position, and (2) ICT is more facile in more polar solvents as would be expected because the polar solvent more effectively accommodates the CT sate. Based on DFT calculations and literature precedent, we would expect the trend in spacer contribution to persist, namely that the alkynyl spacer would be more efficient, followed by the phenyl spacer, and then the direct linkage.

Conclusions

The electronic coupling between a BDP chromophore and a covalently attached electron-donating Carb moiety was tuned through attachment at different positions on the BDP core, specifically the *meso* and *beta* positions, and through the use of various chemical linkers (direct, phenyl spacer, alkynyl spacer). Utilization of the *meso* position for covalent attachment allows several features of the unsubstituted BDP to be retained and supports the consensus in the literature that variation of the linkage between the donor and acceptor moieties can be integral to modulating the photophysical behavior of excited-state deactivation, specifically it can play a role in tuning the rate of charge transfer and eventual recombination. When, however, the *beta* position is used for attachment, more significant modulation of the BDP properties are observed. The *beta*-substituted dyad presents an opportunity to dramatically tune (red shifting) the absorption spectra, while retaining many interesting and desired features of the BDP, specifically stability and high extinction coefficients. However, care must be taken in the design of molecular D-A dyads, in that increasing the conjugation to achieve absorption spectrum tuning can also result in faster CT dynamics. This work provides viable strategies for red shifting absorption of BDP and shows there is a fine balance to be struck in molecular design that motivates future work in this field.

Conflicts of interest

There are no conflicts to declare.

Acknowledgements

ERY thanks the NSF Major Research Instrumentation program for funds that established the multi-user laser facility for transient absorption (CHE-1428633). ST thanks partial support from the U.S Army Research Office (W911NF-15-1-0568).

Notes and references

(1) Lewis, N. S.; Nocera, D. G. *Proc. Natl. Acad. Sci.* **2006**, *103* (43), 15729.
(2) Lin, Y.; Li, Y.; Zhan, X. *Chem. Soc. Rev.* **2012**, *41* (11), 4245–4272.
(3) Chochos, C. L.; Tagmatarchis, N.; Gregoriou, V. G. *RSC Adv.* **2013**, *3*, 7160–7181.
(4) Lin, Y.; Zhan, X. *Mater. Horizons* **2014**, *1* (5), 470–488.
(5) Gust, D.; Moore, T. A.; Moore, A. L. *Acc. Chem. Res.* **2001**, *34* (1), 40–48.
(6) Shoer, L. E.; Eaton, S. W.; Margulies, E. A.; Wasielewski, M. R. *J. Phys. Chem. B* **2015**, *119* (24), 7635–7643.
(7) Dyar, S. M.; Smeigh, A. L.; Karlen, S. D.; Young, R. M.; Wasielewski, M. R. *Chem. Phys. Lett.* **2015**, *629*, 23–28.
(8) Thompson, A. L.; Ahn, T.-S.; Thomas, K. R. J.; Thayumanavan, S.; Martínez, T. J.; Bardeen, C. J. *J. Am. Chem. Soc.* **2005**, *127* (47), 16348–16349.
(9) Ahn, T. S.; Nantalaksakul, A.; Dasari, R. R.; Al-Kaysi, R. O.; Müller, A. M.; Thayumanavan, S.; Bardeen, C. J. *J. Phys. Chem. B* **2006**, *110* (48), 24331–24339.
(10) Nantalaksakul, A.; Mueller, A.; Klaikherd, A.; Bardeen, C. J.; Thayumanavan, S. *J. Am. Chem. Soc.* **2009**, *131* (7), 2727–2738.
(11) Triebs, A.; Kreuzer, F.-H. *Justus Liebig Ann. Chem.* **1968**, No. 718, 208–223.
(12) Ulrich, G.; Ziessel, R.; Harriman, A. *Angew. Chemie Int. Ed.* **2008**, *47* (7), 1184–1201.
(13) Loudet, A.; Burgess, K. *Chem. Rev.* **2007**, *107*, 4891–4932.
(14) Kamkaew, A.; Lim, S. H.; Lee, H. B.; Kiew, L. V.; Chung, L. Y.; Burgess, K. *Chem. Soc. Rev.* **2013**, *42* (1), 77–88.
(15) Liu, J.-Y.; El-Khouly, M. E.; Fukuzumi, S.; Ng, D. K. P. *Chemphyschem* **2012**, *13* (8), 2030–2036.
(16) Liu, J.-Y.; El-Khouly, M. E.; Fukuzumi, S.; Ng, D. K. P. *Chem. Asian J.* **2011**, *6* (1), 174–179.
(17) Wijesinghe, C. A.; El-Khouly, M. E.; Blakemore, J. D.; Zandler, M. E.; Fukuzumi, S.; D'Souza, F. *Chem. Commun.* **2010**, *46* (19), 3301–3303.
(18) Erten-Ela, S.; Yilmaz, M. D.; Icli, B.; Dede, Y.; Icli, S.; Akkaya, E. U. *Org. Lett.* **2008**, *10* (15), 3299–3302.
(19) Kiliolu, T.; Ocak, Y. S. *Microelectron. Eng.* **2011**, *88* (2), 150–154.
(20) Rousseau, T.; Cravino, A.; Bura, T.; Ulrich, G.; Ziessel, R.; Roncali, J. *Chem. Commun.* **2009**, No. 13, 1673–1675.
(21) Suzuki, S.; Kozaki, M.; Nozaki, K.; Okada, K. *J. Photochem. Photobiol. C Photochem. Rev.* **2011**, *12* (4), 269–292.
(22) Roland, T.; Heyer, E.; Liu, L.; Ruff, A.; Ludwigs, S.; Ziessel, R.; Haacke, S. *J. Phys. Chem. C* **2014**, *118* (42), 24290–24301.
(23) Whited, M. T.; Patel, N. M.; Roberts, S. T.; Allen, K.; Djurovich, P. I.; Bradforth, S. E.; Thompson, M. E. *Chem. Commun. (Camb).* **2012**, *48* (2), 284–286.

(24) Kim, S.-Y.; Cho, Y.-J.; Son, H.-J.; Cho, D. W.; Kang, S. O. *J. Phys. Chem. A* **2018**, *122* (13), 3391–3397.
(25) Davis, N. J. L. K.; MacQueen, R. W.; Jones, S. T. E.; Orofino-pena, C.; Cortizo-lacalle, D.; Taylor, R. G. D.; Credgington, D.; Skabara, J.; Greenham, N. C. *J. Mater. Chem. C* **2017**, *5*, 1952–1962.
(26) Kaur, N.; Van Steerteghem, N.; Singla, P.; Kaur, P.; Clays, K.; Singh, K. *Dalton* **2017**, *46*, 1124–1133.
(27) Spiegel, J. D.; Kleinschmidt, M.; Larbig, A.; Tatchen, J.; Marian, C. M. *J. Chem. Theory Comput.* **2015**, *11*, 4316–4327.
(28) Brzeczek, A.; Piwowar, K.; Domagala, W.; Mikolajczk, M. M.; Walczak, K.; Wagner, P. *RSC Adv.* **2016**, *6*, 36500–36509.
(29) Zrig, S.; Re, P.; Andrioletti, B.; Rose, E.; Asselberghs, I.; Clays, K.; Curie-paris, P. M.; De, L.; Uni, K.; Leu, V.; Celestijnenlaan, D.; V, B.-L.; September, R. V. *J. Org. Chem.* **2008**, *73*, 1563–1566.
(30) Maligaspe, E.; Pundsack, T. J.; Albert, L. M.; Zatsikha, Y. V; Solntsev, P. V; Blank, D. A.; Nemykin, V. N. *Inorg. Chem.* **2015**, *54*, 4167–4174.
(31) Ward, M. D. *Chem. Soc. Rev.* **1997**, *26* (5), 365–375.
(32) Wasielewski, M. R. *Chem. Rev.* **1992**, *92*, 435–461.
(33) Lukas, A. S.; Bushard, P. J.; Wasielewski, M. R. *J. Phys. Chem.* **2002**, *106*, 2074–2082.
(34) Huang, G.; Harris, M. A.; Krzyaniak, M. D.; Margulies, E. A.; Dyar, S. M.; Lindquist, R. J.; Wu, Y.; Roznyatovskiy, V. V; Wu, Y.; Young, R. M.; Wasielewski, M. R. *J. Phys. Chem. B* **2016**, *120*, 756–765.
(35) Dance, Z. E. X.; Mickley, S. M.; Wilson, T. M.; Ricks, A. B.; Scott, A. M.; Ratner, M. A.; Wasielewski, M. R. *J. Phys. Chem. A* **2008**, *112*, 4194–4201.
(36) Wasielewski, M. R.; Minsek, D. W.; Niemczyk, M. P.; Svec, W. A.; Yang, N. C. *J. Am. Chem. Soc.* **1990**, *112* (11), 2823–2824.
(37) Weiss, E. A.; Tauber, M. J.; Kelley, R. F.; Ahrens, M. J.; Ratner, M. A.; Wasielewski, M. R. *J. Am. Chem. Soc.* **2005**, *127* (13), 11842–11850.
(38) Hanss, D.; Walther, M. E.; Wenger, O. S. *Coord. Chem. Rev.* **2010**, *254*, 2584–2592.
(39) Ding, F.; Chapman, C. T.; Liang, W.; Li, X. *J. Chem. Phys.* **2012**, *137*, 22A512.
(40) Cave, R. J.; Newton, M. D. *J. Phys. Chem. A* **2014**, *118*, 7221–7234.
(41) Wenger, O. S. *Acc. Chem. Res.* **2011**, *44* (1), 25–35.
(42) Arrigo, A.; Santoro, A.; Indelli, M. T.; Natali, M.; Scandola, F.; Campagna, S. *Phys. Chem. Chem. Phys.* **2014**, *16*, 818–826.
(43) Gilbert, M.; Albinsson, B. *Chem. Soc. Rev.* **2015**, *44*, 845–862.
(44) Popere, B. C.; Della Pelle, A. M.; Thayumanavan, S. *Macromolecules* **2011**, *44* (12), 4767–4776.
(45) Popere, B. C.; Della Pelle, A. M.; Poe, A.; Balaji, G.; Thayumanavan, S. *Chem. Sci.* **2012**, *3*, 3093–3102.
(46) Reddy, G.; Duvva, N.; Seetharaman, S.; D'Souza, F.; Giribabu, L. *Phys. Chem. Chem. Phys.* **2018**, *20*, 27418–27428.
(47) Ooyama, Y.; Hagiwara, Y.; Mizumo, T.; Harima, Y.; Ohshita, J. *New J. Chem.* **2013**, *37*, 2479–2485.
(48) Misra, R.; Jadhav, T.; Dhokale, B.; Gautam, P.; Sharma, R.; Maragani, R.; Mobin, S. M. *Dalt. Trans.* **2014**, *43*, 13076–13086.
(49) Kesavan, P. E.; Gupta, I. *Dalt. Trans.* **2014**, *43*, 12405–12413.
(50) Khetubol, A.; Snick, S. Van; Clark, M. L.; Fron, E.; Coutino-Gonzalez, E.; Cloet, A.; Kennes, K.; Firdaus, Y.; Vlasselaer, M.; Leen, V.; Dehaen, W.; Auweraer, M. Van der. *Photochem. Photobiol.* **2015**, *91*, 637–653.
(51) Sengul, I. F.; Okutan, E.; Kandemir, H.; Astarc, E.; Çosut, B. *Dye. Pigment.* **2015**, *123*, 32–38.
(52) Jadhav, T.; Misra, R.; Biswas, S.; Sharma, G. D. *Phys. Chem. Chem. Phys.* **2015**, *17*, 26580–26588.
(53) Tanriverdi Ecik, E.; Ozcan, E.; Kandemir, H.; Sengul, I. F.; Cosut, B. *Dye. Pigment.* **2017**, *136*, 441–449.
(54) Cheema, H.; Younts, R.; Gautam, B.; Gundogdu, K.; El-shafei, A. *Mater. Chem. Phys.* **2016**, *184*, 57–63.
(55) Gawale, Y.; Adarsh, N.; Kalva, S. K.; Joseph, J.; Pramanik, M.; Ramaiah, D.; Nagaiyan Sekar. *Chem. - A Eur. J.* **2017**, *23*, 6570–6578.
(56) Liao, J.; Zhao, H.; Xu, Y.; Zhou, W.; Peng, F.; Wang, Y.; Fang, Y. *RSC Adv.* **2017**, *7*, 33975–33985.
(57) Liao, J.; Xu, Y.; Zhao, H.; Zong, Q.; Fang, Y. *Org. Electron.* **2017**, *49*, 321–333.
(58) Kesavan, P. E.; Behera, R. N.; Mori, S.; Gupta, I. *J. Fluoresc.* **2017**, *27* (6), 2131–2144.
(59) Maeda, C.; Todaka, T.; Ueda, T.; Ema, T. *Org. Biomol. Chem.* **2017**, *15* (44), 9283–9287.
(60) Kurowska, A.; Brzeczek-Szafran, A.; Zassowski, P.; Lapkowski, M.; Domagala, W.; Wagner, P.; Wagner, K. *Electrochim. Acta* **2018**, *271*, 685–698.
(61) Babu, J.; Ganesan, S.; Karuppusamy, M.; Rajakumar, P. *Chem. Sel.* **2018**, *3*, 9222–9231.
(62) Srinivas, K.; Ramesh, C.; Ananth, M.; Bhanuprakash, K.; Jayathirtha, V.; Giribabu, L. *Synth. Met.* **2011**, *161*, 96–105.
(63) Duvva, N.; Kanaparthi, R. K.; Kandhadi, J.; Marotta, G.; Salvatori, P.; Angelis, F. D. E.; Giribabu, L. *J. Chem. Sci.* **2015**, *127* (3), 383–394.
(64) Brouwer, A. M. *Pure Appl. Chem.* **2011**, *83* (12), 2213–2228.
(65) Dennington, R.; Keith, T.; Millam, J. 2016, p GaussView, Semichem Inc., Shawnee Mission, KS.
(66) Frisch, M. J.; Trucks, G. W.; Schlegel, H. B.; Scuseria, G. E.; Robb, M. A.; Cheeseman, J. R.; Scalmani, G.; Barone, V.; Mennucci, B.; Petersson, G. A.; Nakatsuji, H.; Al., E. 2016.
(67) Becke, A. D. *J. Chem. Phys.* **1993**, *98* (5648–5652).
(68) Lee, C.; Yang, W.; Parr, R. G. *Phys. Rev. B* **1988**, *37* (2), 785–789.
(69) Vosko, S. H.; Wilk, L.; Nusair, M. *Can. J. Phys.* **1980**, *58* (8), 1200–1211.
(70) Stephens, P. J.; Devlin, F. J.; Chabalowski, C. F.; Frisch, M. J. *J. Phys. Chem.* **1994**, *98*, 11623–11627.
(71) Weigend, F.; Häser, M.; Patzelt, H.; Ahlrichs, R. *Chem. Phys. Lett.* **1998**, *294* (1–3), 143–152.
(72) Ditchfield, R.; Hehre, W. J.; Pople, J. A. *J. Chem. Phys.* **1971**,

54 (2), 724–728.

(73) Francl, M. M.; Pietro, W. J.; Hehre, W. J.; Binkley, J. S.; Gordon, M. S.; DeFrees, D. J.; Pople, J. A. *J. Chem. Phys.* **1982**, *77* (7), 3654–3665.

(74) Hehre, W. J.; Ditchfield, K.; Pople, J. A. *J. Chem. Phys.* **1972**, *56* (5), 2257–2261.

(75) Hariharan, P. C.; Pople, J. A. *Theor. Chim. Acta* **1973**, *28* (3), 213–222.

(76) Miertus, S.; Scrocco, S.; Tomasi, J. *Chem. Phys.* **1981**, *55*, 117–129.

(77) Richards, V. J.; Gower, A. L.; Smith, J. E. H. B.; Davies, E. S.; Lahye, D.; Slater (nee Phillips), A. G.; Lewis, W.; Blake, A. J.; Champness, N. R.; Kays, D. L. *Chem. Commun.* **2012**, *48*, 1751–1753.

(78) Ambrose, J. F.; Carpenter, L. L.; Nelson, R. F. *J. Electrochem. Soc.* **1975**, *122* (7), 876–894.

(79) Karon, K.; Lapkowski, M. *J. Solid State Electrochem.* **2015**, *19*, 2601–2610.

(80) Karon, K.; Lapkowski, M.; Juozas, G. *Electrochim. Acta* **2014**, *123*, 176–182.

(81) Lakowicz, J. R. *Principles of Fluorescence Spectroscopy*, 3rd editio.; Springer Science+Business Media, LLC: New York, NY, 2006.

Bodipy-based donor-acceptor dyads were evaluated using transient absorption spectroscopy to reveal the influence of *beta* vs *meso* substitution on excited-state dynamics.

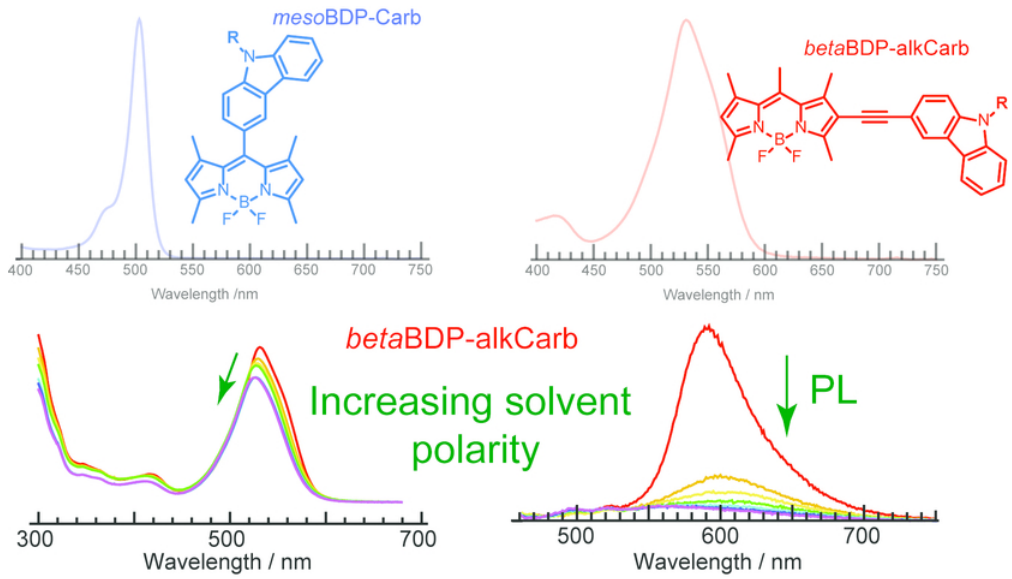

70x40mm (300 x 300 DPI)